Current Mapping Strategy for Improving Two-Terminal Series-Compensated Line Current Differential Protection

Rômulo G. Bainy, Kleber M. Silva, and Brian K. Johnson

***Abstract*—This paper presents a particular case of the generalized alpha plane called current mapping strategy (CMS) formulation applied to differential protection of series-compensated transmission lines. The proposed formulation presents two unique features, control over the internal fault settlement region (FSR) and the use of an operation characteristic (OC). The FSR and the OC are two concentric circles defined on the alpha plane. Additionally, the proposed CMS allows the user to adjust the center and radius of the FSR and OC, according to the desired sensitivity and security of the protection. To validate and test the performance of the improved CMS, numerous computer simulations have been carried out using the Alternative Transients Program (ATP) on a 400 km long series-compensated, 500-kV transmission line. Furthermore, analysis of an extensive database of cases is conducted to highlight the CMS's sensitivity. The obtained results demonstrate the effectiveness of the settings of the CMS and a smooth trajectory to the FSR. The CMS also proved to be stable and reliable even under severe subsynchronous oscillations and outfeed conditions.**

***Keywords*—Power system, protection, differential protection, generalized alpha plane, transmission line, series compensation.**

I. Introduction

OVER the last decade, technological breakthroughs made possible new solutions applied to transmission line protection; the installation of optical fiber composite overhead ground wires enabled the use of differential elements, aiming to implement it as the unitary protection of the line [1]–[3]. For that reason, differential protection of transmission lines became feasible for longer lines, which led to the improvements reported in [4]–[8].

Differential protection of transmission lines commonly consists of phase elements, i.e., ANSI 87LA, 87LB, and 87LC, and negative and zero sequence elements, i.e., ANSI 87LQ and 87LG. The sequence elements have the purpose of detecting asymmetrical faults, even with the occurrence of high fault resistance [5]. On the other hand, the high sensitivity of these elements may lead to maloperations during external faults followed with current transformer (CT) saturation [9]. In addition, an external fault detection algorithm is required to block the operation of sequence elements during external faults. Another advantage of 87LQ and 87LG is that they are more immune to line charging current when compared to phase elements [10]. The performance of transmission line differential protection can be further improved by adaptive method such as [11]. Their strategy consists of restraint areas that change their size in order to improve dependability and sensitivity of the phase elements.

In [12], a complete protection scheme of line differential elements based on the alpha plane is presented in detail, where the advantages were established through careful testing. Although the operational plane is presented as a graphical representation of the differential element operation, the alpha-plane is also a valuable tool. The complex variable gamma consists of the ratio between local and remote currents of a transmission line and is calculated for each phase. An innovative restraint characteristic using the alpha plane, called "rainbow," is presented in [10] [13]. Their approach enables great performance during CT saturation. Furthermore, the restraint characteristic can be intuitively adjusted according to the unique behavior of the transmission line protection. Likewise, problems such as CT saturation and channel asymmetry are better faced by the rainbow restraint characteristic, leading to reliable and secure operation of the differential protection. An adaptive approach for the alpha plane and the restraining characteristic is presented by [14]. One of the main benefits is the enhanced performance against high impedance faults.

Transmission line series compensation usually varies from 25% to nearly 100%; some advantages are the increased power transfer capability and improved power system stability [1], [15]–[17]. A downside of series-compensated transmission lines are the challenges imposed on traditional protection schemes [18]. The series capacitors can be installed either at line ends or at a central location [19]. The former is more common and results in challenges to the protection of the transmission lines. The capacitor bank internal overvoltage protection uses metal oxide varistors (MOV) [20]. This nonlinear resistance is installed in parallel with the capacitor banks to limit the overvoltage across the capacitors [21]. However, the MOV has limited energy absorption; therefore, a flash over path, such as a triggered air gap in conjunction with a bypass circuit breaker is required to avoid MOV failure [21].

Series compensated transmission lines pose challenges for directional, distance, and differential protection because the transient behavior of the series capacitor is not readily predictable [22]. For example, distance protection may fail to operate due to signal inversions; large errors may be caused by sub-synchronous oscillations [17]. Voltage inversion in the case of faults near a series capacitor may cause the relay

R. G. Bainy and B. K. Johnson are with the University of Idaho, Moscow, ID 83844-1023 USA (e-mail: r.bainy@ieee.org and b.k.johnson@ieee.org).

Kleber M. Silva is with the University of Brasilia, Brasília, DF 70910-900, Brazil (e-mail: klebermelo@unb.br).

Paper submitted to the International Conference on Power Systems Transients (IPST2021) in Belo Horizonte, Brazil, June 6–10, 2021.

to not operate in case of internal faults [15]. In addition, reduced zone 1 reach settings are require for distance elements, increasing the reliance of communication assisted overreaching distance schemes. Directional and differential elements are severely affected current inversion. Such a condition is extremely rare and occurs when the equivalent impedance from the source to the fault is capacitive and the remaining impedance from the fault to the remote terminal is inductive [15]. Other downsides are the increase of short-circuit levels and potential subsynchronous resonance with steam turbine generators [22]. Furthermore, the impedance calculated by the distance element can be incorrect if the capacitor bank is not bypassed during an internal fault, and phasor-based protection can face errors on phasor estimation during subsynchronous resonance [22]. Previous efforts have tried to improve the performance of differential protection of series-compensated transmission lines. The authors of [23] combined instantaneous values with a moving window averaging technique to increase sensitivity for the high-resistance internal faults.

This paper presents a current mapping strategy that improves the performance of the alpha plane line current differential element for use in series-compensated transmission line protection. The formulation allows different settings, e.g., the user can adjust the CMS for improved sensitivity or enhanced security. The performance of the element is tested through transient and parametric analysis with a massive number of fault and system conditions.

II. CMS FORMULATION

The CMS proposed in this paper is a particular case of the generalized plane presented in [24]. Considering a two-terminal transmission line, the differential current, $\bar{I}_{dif}$, and restrain current, I_{res}, are defined as:

$$\bar{I}_{dif} = \bar{I}_L + \bar{I}_R = I_{dif,re} + jI_{dif,im} \quad (1)$$

$$I_{res} = |\bar{I}_L| + |\bar{I}_R| \quad (2)$$

where the math accent ($\bar{}$) represents a phasor quantity; R and L are the remote and local terminals, respectively; $\bar{I}$ is the phasor of current measured at terminal i; the subscripts re and im represent its real and imaginary parts; and the j-operator has a value exactly equal to $\sqrt{-1}$.

Next, we defined the differential and restraint currents of the CMS, as:

$$\bar{I}_{dif,eq} = \bar{I}_M + \bar{I}_N \quad (3)$$

$$\bar{I}_{res,eq} = \eta_1\bar{I}_M - \eta_2\bar{I}_N \quad (4)$$

where $\bar{I}_{dif,eq}$ and $\bar{I}_{res,eq}$ are the differential current and restraint current of the CMS, respectively; η_1 and η_2 are the adjustment factors; and I_M and I_N are defined below.

The equivalence between the original currents and the CMS currents is guaranteed by two assumptions: 1) the differential currents of both ($\bar{I}_{dif,eq}$ and $\bar{I}_{dif}$) are equal, and 2) the restraint currents of both ($\bar{I}_{res,eq}$ and I_{res}) are equal. Thus, a linear system of equations can be obtained from (1)-(4).

$$\begin{bmatrix} 1 & 0 & 1 & 0 \\ 0 & 1 & 0 & 1 \\ \eta_1 & 0 & -\eta_2 & 0 \\ 0 & \eta_1 & 0 & -\eta_2 \end{bmatrix} \cdot \begin{bmatrix} I_{M,re} \\ I_{M,im} \\ I_{N,re} \\ I_{N,im} \end{bmatrix} = \begin{bmatrix} I_{dif,re} \\ I_{dif,im} \\ I_{res} \\ 0 \end{bmatrix} \quad (5)$$

Since (5) is an exactly determined and consistent linear system, its solution is straightforwardly obtained, whereby the currents $\bar{I}_M$ and $\bar{I}_N$ of the equivalent device are computed as:

$$\bar{I}_M = \frac{1}{\eta_1+\eta_2}\left(\eta_2\bar{I}_{dif} + I_{res}\right) \quad (6)$$

$$\bar{I}_N = \frac{1}{\eta_1+\eta_2}\left(\eta_1\bar{I}_{dif} - I_{res}\right) \quad (7)$$

Finally, $\bar{I}_M$ and $\bar{I}_N$ are combined as (8) to obtain the complex variable Γ, which is plotted in the alpha plane for each phase.

$$\Gamma = \frac{\bar{I}_M}{\bar{I}_N} = \frac{\eta_2\bar{I}_{dif} + I_{res}}{\eta_1\bar{I}_{dif} - I_{res}} = \Gamma_{re} + j\Gamma_{im} \quad (8)$$

Equation (8) can be divided in its real and imaginary parts, as shown in (9) and (10), respectively.

$$\Gamma_{re} = M_{re}\left(\frac{|\bar{I}_{dif}|^2 + I_{res}f(\eta_1,\eta_2)}{|\bar{I}_{dif}|^2 + I_{res}f(-\eta_2,\eta_2)}\right) \quad (9)$$

$$\Gamma_{im} = M_{im}\left(\frac{I_{res}I_{dif,im}}{|\bar{I}_{dif}|^2 + I_{res}f(-\eta_2,\eta_2)}\right) \quad (10)$$

where M_{re}, M_{im}, $f(\eta_1,\eta_2)$, and $f(-\eta_2,\eta_2)$ can be defined as:

$$M_{re} = \frac{\eta_2}{\eta_1} \quad (11)$$

$$M_{im} = \eta_2 + \frac{\eta_2^2}{\eta_1} \quad (12)$$

$$f(\eta_1,\eta_2) = -\eta_1\eta_2 I_{res} + (\eta_1-\eta_2)I_{dif,re} \quad (13)$$

$$f(-\eta_2,\eta_2) = \eta_2^2 I_{res} - 2\eta_2 I_{dif,re} \quad (14)$$

We can further organize these expressions by creating two adjustments for the protection elements called Γ_f and k_Δ. Considering $\Gamma_f = M_{re}$ and $k_\Delta = M_{im}M_{re}$, the system of equations can be solved and expressions for η_1 and η_2 in terms of Γ_f and k_Δ are obtained as (15) and (16), respectively.

$$\eta_1 = \frac{1}{k_\Delta}\left(1+\Gamma_f\right) \quad (15)$$

$$\eta_2 = \Gamma_f \cdot \eta_1 \quad (16)$$

The overall behavior of the CMS in the alpha plane is shown in Fig. 1. The pre-fault is fixed at the point $(-1;0)$. The circular FSR is adjustable according to Γ_f and k_Δ; Γ

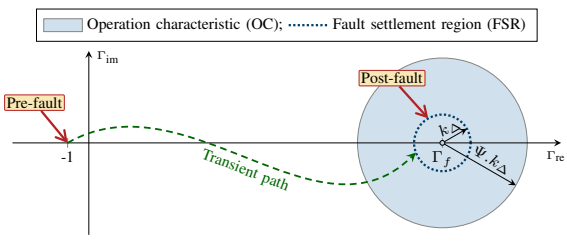

Fig. 1. Behavior of the CMS in the alpha plane.

will settle at the border of the FSR if an internal fault occurs. The circular operation characteristic (OC) is defined around the FSR. The OC radius ($\Psi \cdot k_\Delta$) is adjusted according to the desired sensitivity and speed, where the greater the product is, the faster and more sensitive the element will be. The transient path depends on the pre-fault (e.g., load current) and fault (e.g., fault inception angle) conditions. The CMS allows multiple adjustments for Γ_f, k_Δ, and Ψ, which enable settings with emphasis on sensitivity, speed, or security. Smaller values of Γ_f and k_Δ increase the security [24]. The CMS is also a good alternative in case negative/zero sequence currents are not available.

The CMS can improve the line differential protection performance by enabling the adjustments Γ_f and k_Δ. Fig. 2 shows a flowchart as an example of a protection scheme that utilizes the CMS. The measured currents synchronized in time at each end of the line (local and remote) are fed to the phasor calculation block. The differential and restrain currents ($\bar{I}_{dif}$ and I_{res}) are calculated for each phase and then sent to the CMS block. The mapped currents $\bar{I}_M$ and $\bar{I}_N$ are then used to calculate Γ by (8). A trip signal is sent if Γ settles inside the operation characteristic for more than a half a cycle (or 8 samples).

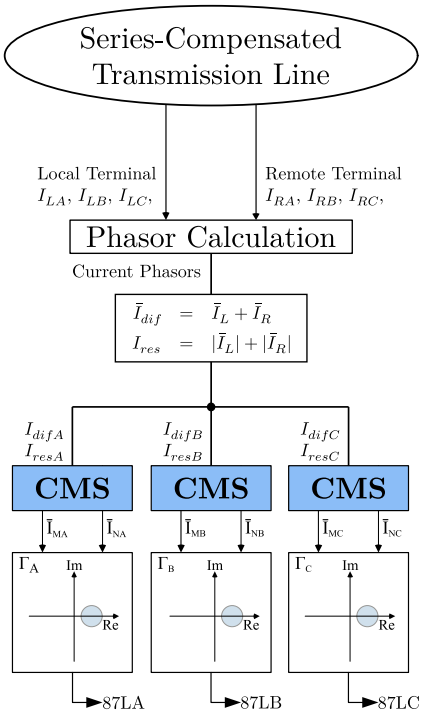

Fig. 2. Flowchart of Transmission Line Protection using the CMS

III. Performance Evaluation

The advantages of using the CMS to protect series-compensated transmission lines are highlighted by comparing CMS's performance against the regular alpha plane (herein called AP). The adjustments Γ_f, k_Δ, and Ψ directly affect the security, speed, and sensitivity of the element. Furthermore, the adjustments can be set according to the desired emphasis. The CMS was tested for the two sets of adjustments shown in Table I.

TABLE I
Chosen CMS adjustments for tests

Adjustment	Γ_f	k_Δ	Ψ	$\Psi \cdot k_\Delta$	Emphasis
CMS-A1	10	0.2	25	5	Sensitivity
CMS-A2	2	0.4	5	2	Security

The CMS-A1 enables high sensitivity, while CMS-A2 provides enhanced security. The OC radius ($\Psi \cdot k_\Delta$) of the CMS-A1 and CMS-A2 are set to 5 and 2, respectively; therefore CMS-A1 will be faster and more sensitive than CMS-A2. The offset from the pre-fault point (-1;0) is defined by Γ_f, the CMSs A1 and A2 are set to 10 and 2, respectively; therefore, the CMS-A2 will be more secure than the CMS-A1. Both have a harmonic restraining restriction as show in (17) always enabled in order to improve security during situations such as external faults with CT saturation.

$$I_{res} = \sum_{i=1}^{\tau} |\bar{I}_i| + f \cdot k_h \left(\sum_{i=1}^{\tau} |\bar{I}_{i,h}| \right) \tag{17}$$

Each adjustment of CMS is compared to the AP side-by-side in terms of their performance for series-compensated transmission line protection. The AP consists of the ratio between local and remote currents measured on the ends of the transmission line: $\Gamma_{AP} = \frac{\bar{I}_L}{\bar{I}_R}$. The variable Γ_{AP} is plotted in the alpha-plane and the "rainbow" restraint characteristic is used [13]. The studies are summarized in two different categories: transient analysis plus analysis of a massive number of cases with varying fault conditions.

The system consists of a 400 km, 500 kV transmission line with the series compensation set to 70% and the shunt reactor compensation set to 60%. The source impedance and transmission line parameters are given in the Appendix. The source impedance ratio (SIR) will be varied to explore the impact on element performance. The series compensation is achieved by two fixed Series Capacitor Banks (SCB) installed at the ends of the transmission line. The shunt compensation is achieved by one fixed Shunt Reactor Bank (SRB) installed at each end line terminal. The CT was specified as C800 2000-5A, and modeled as proposed by the IEEE Power System Relaying Committee in [25]. The CCVT was sized and modeled as specified in [26]. The charging current drawn by transmission line capacitance was estimated and charging current compensation for the differential element was determined following the procedure performed by [10]. The Appendix presents the value of all the parameters.

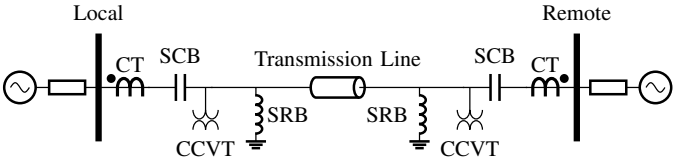

Fig. 3. 500 kV 400km series-compensated transmission line

The capacitor bank is divided in three single-phase banks

which are individually protected, as shown in Fig. 4. The scheme utilizes a MOV and a triggered gap to provide SCB protection. The MOVs are simulated as an the exponential current-dependent resistor type 92, while the triggered gap utilized the Transient Analysis of Control Systems (TACS) switch Type 13, both available in ATP/ATPDraw. The logic of the triggered gap firing control was implemented using the MODELS environment in ATPDraw, and is based on monitoring the current and absorbed energy by the MOV, called I_{MOV} and E_{MOV}, respectively. The Appendix presents these parameters and the curve of the MOVs.

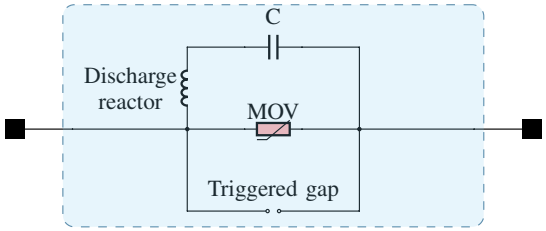

Fig. 4. Capacitor bank with MOV and triggered gap installed in all phases

A. Transient Analysis

Case 1 illustrates an internal solid single-line-to-ground fault (AG) 360 km far away from the local terminal (i.e., 90% of the transmission line length). Such a scenario led to the operation of the SCB overvoltage protection at the remote terminal, where the capacitor was bypassed by the MOV and then by the triggered gap (6 ms and 10 ms after the fault, respectively). The currents seen at the Local and Remote terminals are shown in Fig. 6a and Fig. 6b, respectively. The results for the alpha plane are shown in Fig. 5a. The subsynchronous frequency components (SSC) can be seen at the local terminal clearly in Fig. 6a. However, the same cannot be said about the remote terminal in this case because the capacitor was bypassed, first by the MOV and then by the triggered gap. The results for CMS-A1 and CMS-A2 considering their operation characteristic and the adjusted FSR are shown in Fig. 5a. One can observe that the subsynchronous frequency components did not affect the proposed CMS performance. Moreover, the proposed CMS formulation proved reliable and only the phase A element issued a trip command. The AP, on the other hand, oscillated around a point in the alpha plane due to SSC which represents a risk of failing to trip if the Γ_{AP} returns to the restraint characteristic. Case 2 presents an internal 250 Ω single-line-to-ground fault (BG) at the midpoint

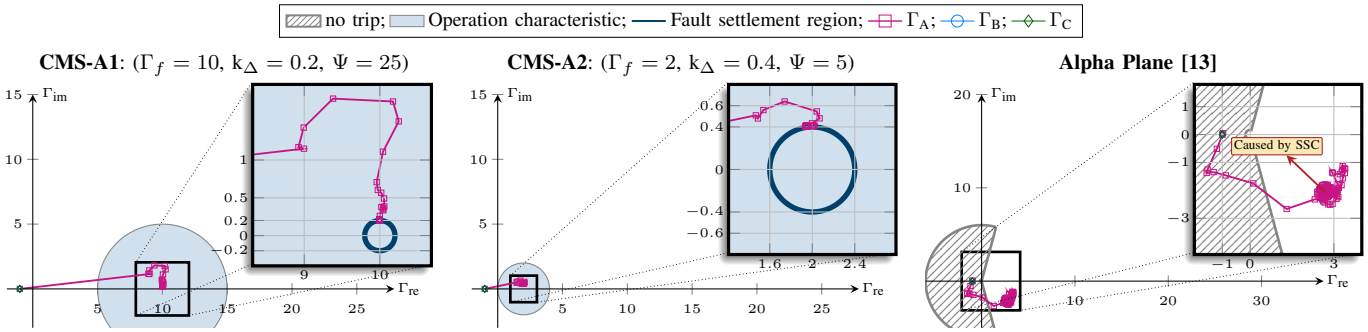

(a) Case 1: Internal single-phase fault AG with subsynchronous components (SSC)

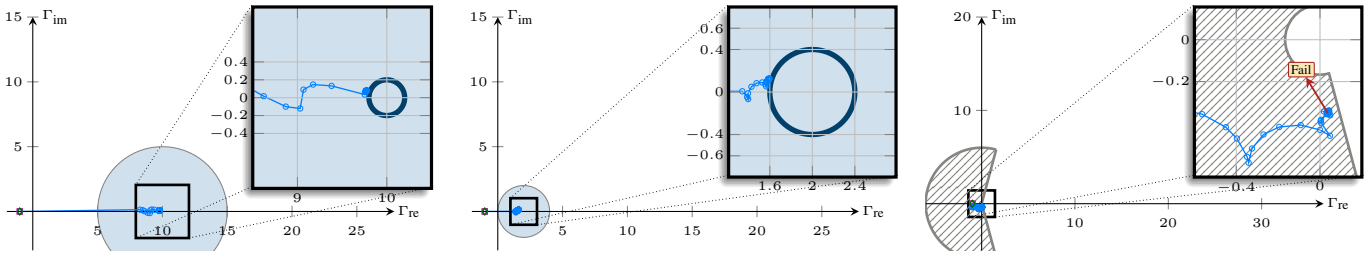

(b) Case 2: Internal single-phase fault BG with outfeed

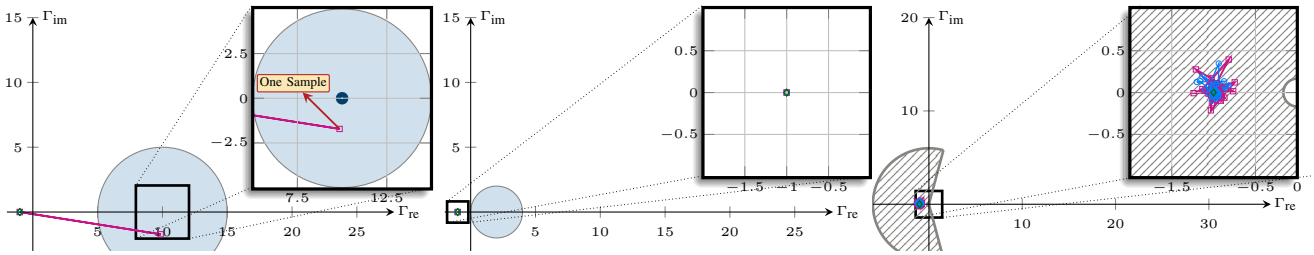

(c) Case 3: External three-phase fault

Fig. 5. Comparison of protection performance between two settings for the CMS and the alpha plane for difference fault conditions

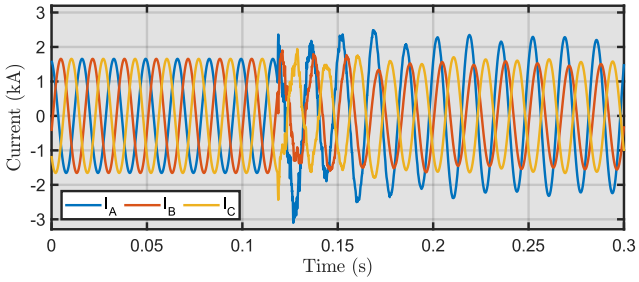

(a) Local terminal (primary currents)

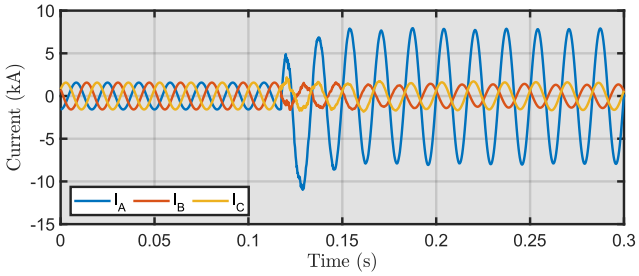

(b) Remote terminal (primary currents)

Fig. 6. Sub-synchronous frequency components for Case 1

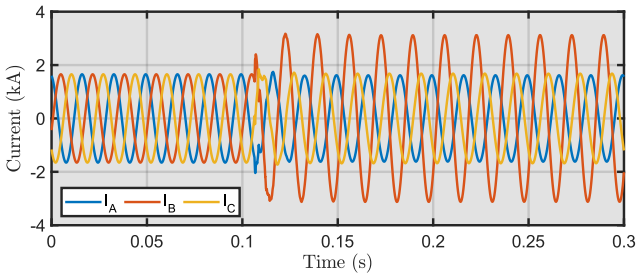

(a) Local Current

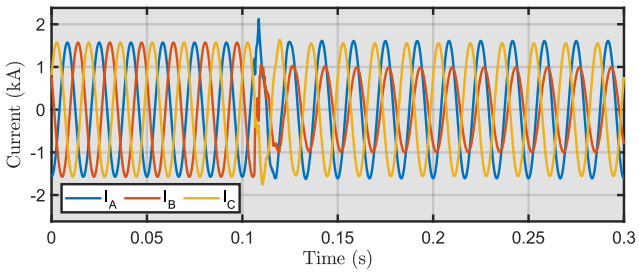

(b) Remote Current

Fig. 7. Outfeed condition components for Case 2

of the transmission (i.e., 50% of the transmission line length). Such a scenario resulted in an outfeed condition [3] at the remote terminal which can be seen on Fig. 7b which represents a challenge for the line protection scheme. The currents measured at the remote terminal went down during the fault. The results for the alpha plane are shown in Fig. 5b. One can observe that both sets of adjustments for the CMS successfully detected and issued a trip for the phase B, however the conventional AP failed to operate. Therefore, the CMS can be advantageous when compared to the AP in regards to outfeed conditions.

Case 3 presents an external three-phase fault (ABC) at the local terminal of the transmission (i.e., before the local CTs of the transmission line). Such a scenario resulted in the bypass of the local and remote capacitor banks 300 ms after the fault. The currents measured at both terminals went down after the capacitor banks were bypassed. The results for the alpha plane are shown in Fig. 5c. One can observe that the CMS-A1 and the AP were fairly affected by such condition. On the other hand, the CMS-A2 (settings with enhanced security) was not affected by the external fault followed by the bypass of the capacitor banks. Even though the two CMSs and the AP presented different responses, none of them misoperated.

B. Parametric Analysis

The results of the parametric analysis with a massive number of fault and system conditions are presented in terms of trajectories [12] in the alpha plane. A total of three cases, with different sets of parameters varied, presented in Fig. 8. Each case examines the CMS performance against the variation of fault location, fault resistance, SIR, load current, and fault type, whereas the simulation parameters follow the defined boundaries listed in Table II.

TABLE II
RANGE OF PARAMETERS FOR THE PARAMETRIC ANALYSIS

Simulation Variables	**Range**
Load (δ)	-15, -14,..,+14, +15 (°)
SIR_{L1}	0.063, 0.08, 0.1, 0.2,...,1.0
SIR_{R1}	0.063, 0.08, 0.1, 0.2,...,1.0
Fault Location (d)	1, 5, 10,..,90, 95, 99 (% of the TL)
Type of fault	AG,..., AB,..., ABG, ABC
Fault Resistance (Ω)	phase-to-phase: 0, 5,..,195, 200
	phase-to-ground: 0, 10,..,90, 1000

Case 4 studies the effects of the load and the SIR variation on both ends of the transmission line. A total of 770 simulations were performed and the CMS successfully operated for all imposed conditions. Moreover, the two sets of adjustments resulted in the FSR defined by k_Δ and Ψ. On the other hand, the AP failed in 99 simulations related to conditions where the elevated SIR (i.e., weaker sources at one end or the other) resulted in smaller fault currents. Therefore, the CMS proved to be more sensitive than the AP in respect to different source strengths. Fig. 8a shows the response of the different elements in the alpha plane.

Case 5 presents the analysis of different fault locations over the protection. The most common types of faults are covered for three load conditions for a total of 340 simulations. The CMS operated correctly for all imposed conditions, in addition to maintaining a coherent FSR. In regards to the AP, a total of 43 fault conditions resulted in failure to operate. As in Case 3 the performance AP was less sensitive than the proposed CMS. Case 6 presents a study of the influence of fault resistance, where values up to 200 Ω and 1000 Ω were studied for phase-to-phase and phase-to-ground resistances, respectively. An interesting aspect of Case 5 is that it highlights one of the advantages of having the different adjustments (i.e., Γ_f and

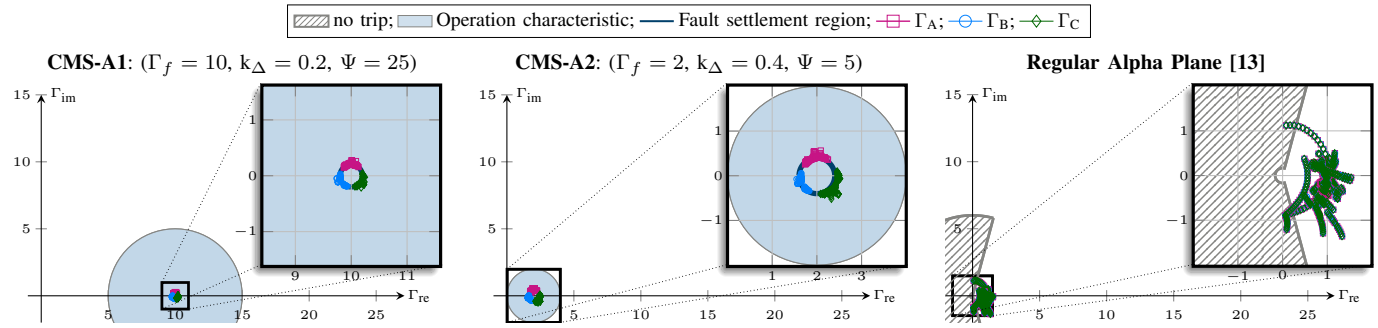

(a) Case 4: Massive Data Analysis - load and SIR (770 simulations)

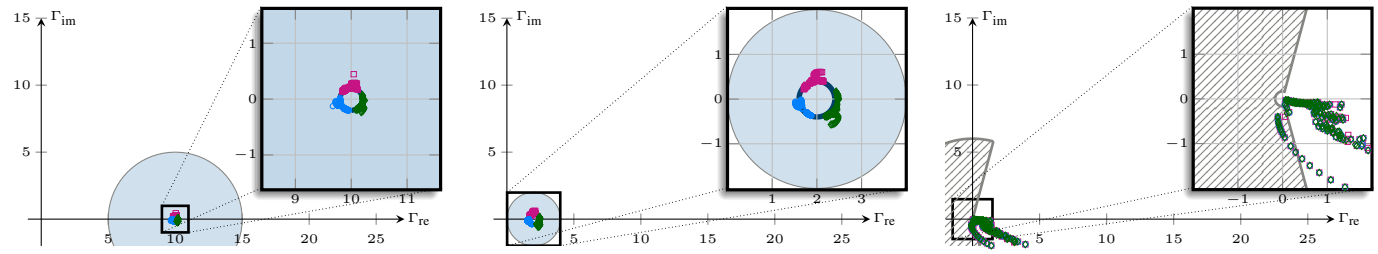

(b) Case 5: Massive Data Analysis - location (340 simulations)

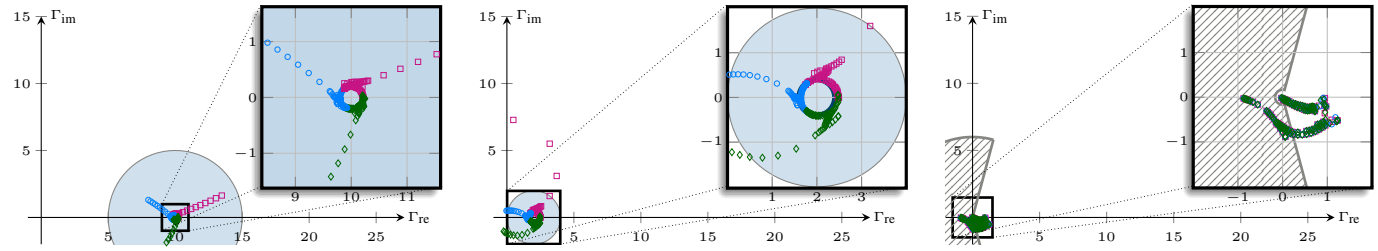

(c) Case 6: Massive Data Analysis - Fault Resistance (230 simulations)

Fig. 8. Series-compensated transmission line protection using CMS and regular alpha plane

k_Δ) enabled by the proposed formulation. The CMS-A1 was adjusted aiming for improved sensitivity, therefore it operated even under high impedance faults. On the other hand, the CMS-A2 was set to be more secure causing it to not operate for 16 conditions out of 230. Again, the AP was not sensitive enough and failed to operate for 117 simulations, as shown in Fig. 8b. A summary of the performance of the tested algorithms is presented in Fig. 9 and Table III. The condition that resulted in more problems for the CMS and the AP was the fault resistance. The AP failed for 259 of 1340 simulations, a 19% fail rate. The two adjustments of the proposed CMS-A2 only failed for 16 simulations, or 1.2% of all simulations. The CMS-A1 element did not have any misoperations.

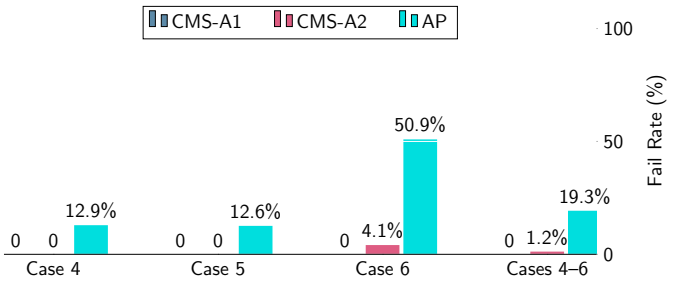

Fig. 9. Fail rate of the CMS and the AP for cases 4, 5, and 6

TABLE III
SUMMARY OF THE ELEMENT PERFORMANCE OVER CASES 4, 5, AND 6

Algorithm	Cases			
	4	5	6	Total
CMS-A1	0	0	0	0
CMS-A2	0	0	16	16
AP	99	43	117	259

C. Effect of Different Ratios of Series Compensation

In order to study the effects of the compensation ratio over the CMS, the capacitor banks of the line shown in Fig. 3 were tuned to compensate 55% and 85% of the lines impedance. Case 7 studies the 55% compensation where each series capacitor bank is tuned to $j21.9\,\text{m}\mho$. Case 8 presents compensation of 85% and each series capacitor bank is set to $j33.9\,\text{m}\mho$. The results for cases 7 and 8 are shown in Figures 10a and 10b, respectively. They present a total of 1340 simulations each with different initial and fault conditions, according to the defined boundaries presented in Table II.

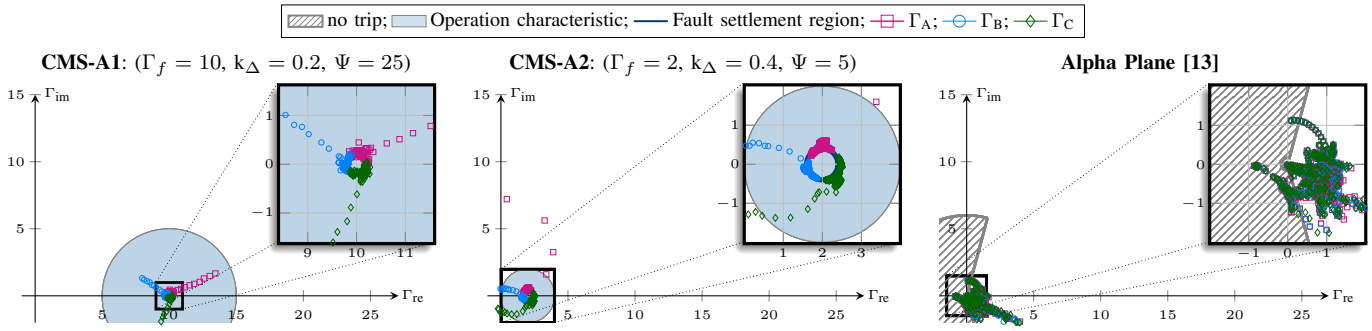

(a) Case 7: Massive Data Analysis - Compensation at 55% (1340 simulations)

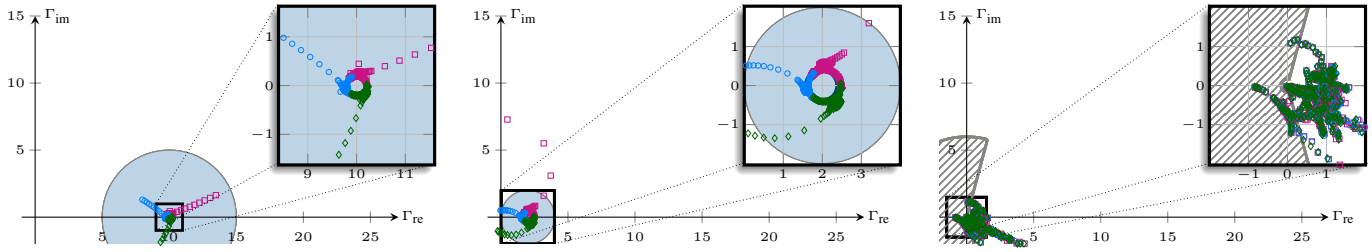

(b) Case 8: Massive Data Analysis - Compensation at 85% (1340 simulations)

Fig. 10. Comparison of protection performance between two settings for the CMS and the alpha plane for different compensation ratios

One can observe that Figures 10a and 10b are extremely similar; therefore different compensation ratios did not affect the performance of the CMS. Additionally, cases 7 and 8 present equivalent results to the ones shown in Fig. 9 and Table III.

IV. Conclusions

This paper presented and thoroughly tested a new current mapping strategy formulation for a series-compensated transmission line. One of the benefits is the adjustable circular fault settlement region in the alpha plane where the Γ settles if an internal fault occurs. The user only needs to set three parameters named Γ_f, k_Δ, and Ψ. The sensitivity and security of the CMS can be either improved or reduced depending on the value of the three parameters. Therefore, the settings can be adjusted in a straightforward fashion according to the desired emphasis (sensitivity or security). The solution's effectiveness was proven by the performed transient and through 1340 cases with varying system and fault conditions. The CMS was tested for three different compensation ratios of the line, and the results shown that the formulation was not affected. The cases were systematically compared with the regular alpha plane [13]; the CMS correctly operated for all the simulations while the regular alpha plane failed for 19.3% of all cases. Future works will include studies for double-circuit transmission lines with series compensation and effects of ferroresonance on the CMS. Additionally, an adaptive CMS formulation is also being developed by the authors and will be presented in future publications.

V. Appendix

The parameters of the series-compensated transmission line simulated in this paper are presented in Table IV. The series capacitor banks simulated on cases 7 and 8 were set to $j21.9\,\text{m}\mho$ and $j33.9\,\text{m}\mho$, respectively.

TABLE IV
Power System Simulation Data

Transmission Line			
Y_{TL0}	$j2.89\ \mu\mho$/km	Z_{TL0}	$0.493 + j2.89\ \Omega$/km
Y_{TL1}	$j6.12\ \mu\Omega$/km	Z_{TL1}	$0.018 + j0.267\ \Omega$/km
l_{TL}	400 km		
Series Capacitors and Shunt Reactors Bank			
B_{SCB}	$j27949\ \mu\mho$	X_{SRB}	$1331\ \Omega$

The parameters of the equivalent sources of local and remote (L and R) are shown below:

$$Z_{i0} = SIR_{i0} \cdot Z_{TL0} \cdot l_{LT} \quad (18)$$

$$Z_{i1} = SIR_{i1} \cdot Z_{TL1} \cdot l_{LT} \quad (19)$$

$$SIR_{i0} = 0.101 \quad (20)$$

$$SIR_{i1} = 0.063 \quad (21)$$

where i is equal to L and R.

The energy and current trigger values for local and remote triggered gaps are listed in Table V varying according to the compensation ratio.

TABLE V
Settings of Local and Remote Triggered Gaps

Data	70%	55%	85%
E_L [MJ]	63.8	94.9	55.9
I_L [kA]	7.32	8.74	6.2
E_R [MJ]	64.2	95.3	56.2
I_R [kA]	7.3	8.8	6.22

The MOVs of local and remote terminal follow the arrester data in Table VI.

TABLE VI
MOV ARRESTER MODEL DATA

I[A]	U[V] (Local)	U[V] (Remote)
0.00011	68462.5	68453.75
5.9	109540	109526
1,000	136925	136907.5

REFERENCES

[1] H. J. Altuve and E. O. Schweitzer, *Modern Solutions for Protection, Control and Monitoring of Electric Power Systems*, 1st ed. Pullman, USA: Quality Books, 2010.

[2] G. Ziegler, *Numerical Differential Protection: Principles and Applications*, 2nd ed. Berlin, Germany: Siemens, 2012.

[3] M. Hossain, I. Leevongwat, and P. Rastgoufard, "Revisions on alpha plane for enhanced sensitivity of line differential protection," *IEEE Transactions on Power Delivery*, vol. 33, no. 6, pp. 3260–3262, Dec 2018.

[4] G. Benmouyal and T. Lee, "Securing Sequence-Current Differential Elements," in *31st Annual Western Protective Relay Conference*, Spokane, Washington, 2004.

[5] G. Benmouyal and J. B. Mooney, "Advanced Sequence Elements for Line Current Differential Protection," in *33rd Annual Western Protective Relay Conference*, 2006.

[6] Z. Y. Xu, Z. Q. Du, L. Ran, Y. K. Wu, Q. X. Yang, and J. L. He, "A Current Differential Relay for a 1000-kV UHV Transmission Line," *IEEE Transactions on Power Delivery*, vol. 22, no. 3, pp. 1392–1399, July 2007.

[7] Y. Xue, D. Finney, and B. Le, "Charging Current in Long Lines and High-Voltage Cables – Protection Application Considerations," in *39th Annual Western Protective Relay Conference*, 2013.

[8] B. Kasztenny, N. Fischer, and H. J. Altuve, "Negative-sequence differential protection - principles, sensitivity, and security," in *68th Annual Conference for Protective Relay Engineers*. IEEE, 2015, pp. 364–378.

[9] H. Miller, J. Burger, N. Fischer, and B. Kasztenny, "Modern line current differential protection solutions," in *2010 63rd Annual Conference for Protective Relay Engineers*. Spokane, WA, USA: IEEE, March 2010.

[10] B. Z. Kasztenny, G. Benmouyal, H. J. Altuve, and N. Fischer, "Tutorial on Operating Characteristics of Microprocessor-Based Multiterminal Line Current Differential Relays," in *38th Annual Western Protective Relay Conference*, no. November 2011. Schweitzer Engineering Laboratories, 2011, pp. 1–30.

[11] S. Dambhare, S. A. Soman, and M. C. Chandorkar, "Adaptive Current Differential Protection Schemes for Transmission-Line Protection," *IEEE Transactions on Power Delivery*, vol. 24, no. 4, pp. 1832–1841, Oct 2009.

[12] G. Benmouyal, *The Trajectories of Line Current Differential Faults in the Alpha Plane*, Schweitzer Engineering Laboratories, Pullman, WA, 2005.

[13] H. J. Altuve, G. Benmouyal, J. Roberts, and D. A. Tziouvaras, "Transmission line differential protection with an enhanced characteristic," in *Eighth IEE International Conference on Developments in Power System Protection*, vol. 2004, no. 1. IET, 2004, pp. 414–419.

[14] S. Sarangi and A. K. Pradhan, "Adaptive α-plane line differential protection," *IET Generation, Transmission Distribution*, vol. 11, no. 10, pp. 2468–2477, July 2017.

[15] P. M. Anderson and R. G. Farmer, *Series Compensation of Power Systems*. PBLSH! Incorporated, 1996.

[16] P. Kundur, *Power System Stability and Control*. McGraw-Hill, 2006.

[17] B. Kasztenny and G. Brunello, "Distance Protection of Series-Compensated Lines: Problems and Solutions," in *2002 Transmission and Distribution Latin American Conference*, no. March, Sao Paulo, 2002.

[18] G. Corpuz, K. Koellner, J. Bell, S. Rajan, A. Somani, and M. Thompson, "Series-compensated line protection challenges in the CREZ region," *2014 67th Annual Conference for Protective Relay Engineers, CPRE 2014*, pp. 664–675, 2014.

[19] *IEEE Standard for Series Capacitor Banks in Power Systems*, IEEE Std 824-2004 Std., May 2005.

[20] *IEEE Guide for the Functional Specification of Fixed-Series Capacitor Banks for Transmission System Applications*, IEEE Std 1726-2013 Std., Dec. 2014.

[21] Y. Xue, B. Kasztenny, D. Taylor, and Y. Xia, "Series compensation, power swings, and inverter-based sources and their impact on line current differential protection," in *2013 66th Annual Conference for Protective Relay Engineers*, 2013, pp. 80–91.

[22] H. J. Altuve, J. B. Mooney, and G. E. Alexander, "Advances in series-compensated line protection," in *2009 62nd Annual Conference for Protective Relay Engineers*, 2009, pp. 263–275.

[23] S. Dambhare, S. A. Soman, and M. C. Chandorkar, "Current differential protection of transmission line using the moving window averaging technique," *IEEE Transactions on Power Delivery*, vol. 25, no. 2, pp. 610–620, April 2010.

[24] R. G. Bainy and K. M. Silva, "Enhanced generalized alpha plane for numerical differential protection applications," *IEEE Transactions on Power Delivery (Early Access)*, pp. 1–1, 2020.

[25] *EMTP Reference Models for Transmission Line Relay Testing*, IEEE Power System Relaying Committee, 2004.

[26] E. Pajuelo, G. Ramakrishna, and M. S. Sachdev, "Phasor estimation technique to reduce the impact of coupling capacitor voltage transformer transients," *IET Generation, Transmission & Distribution*, vol. 2, no. July 2007, pp. 588–599, 2008.

Rômulo G. Bainy received the Ph.D. degree from the University of Brasília (UnB), Brazil in 2019. He was a visiting scholar in Washington State University, Pullman, USA, in 2018. His research interests are in power system protection, fault location, electromagnetic transients, renewable energy, and CCVTs. He is a reviewer for IEEE Transactions journals and IEEE conferences.

Dr. Bainy is a Postdoctoral Fellow in the University of Idaho, Moscow, USA.

Kleber M. Silva received the B.Sc., M.Sc., and Ph.D. degrees in electrical engineering from the University of Campina Grande, Brazil, in 2004, 2005, and 2009, respectively. Since 2009, he has been a Professor with the University of Brasília, Brasília, Brazil, and the Head of the Power System Protection Group. He is an Editor for the IEEE Transactions on Power Delivery and Member of SC B5—Protection and Automation Committee of Cigre Brazil. His research interests are on power system protection, fault location, and electromagnetic transients.

Brian K. Johnson received his doctoral degree in EE at the University of Wisconsin-Madison in 1992. He is the Schweitzer Engineering Laboratories Endowed Chair in Power Engineering and a Professor in the University of Idaho ECE Department. His interests include power systems applications of power electronics, power system protection, and power system transients.

Dr. Johnson is a registered professional engineer in the State of Idaho.